Yehia et al.
Medical Journal of Cell Biology 2022
DOI: 10.2478/acb-2022-0002
Received: 28.01.2022
Accepted: 2.03.2022

Silica nanoparticles in targeted human cancer therapy

Hesham Mohamed Abdal-Salam Yehia[1], Said Mahmoud Said[1], Noheer Galal Elden Rashad Ragb[2]

Abstract

One of the leading causes of death across the world is cancer. Despite massive attempts to develop efficient chemotherapy medications, there is still a significant toxicity and selectivity problem. We are looking for novel therapies and preventative strategies due to the toxicity of contemporary chemotherapy and cancer cell resistance to anticancer drugs. The structure and molecular characteristics of Na2SiO3 nanoparticles were investigated using density-functional theory calculations at the B3LYP/6-311G** level. The study looked at engineering qualities and several molecular recipes like HOMO, LUMO, and Egap in order to figure out how to arrange molecules as a powerful antioxidant, and hence the majority of the compounds are anticancer. We discovered that Na2SiO3 gel particles are responsible for antioxidant activity, implying that it can be employed as an antioxidant and anticancer for cancer prevention and treatment.

Running title: Silica nanoparticles in targeted human cancer

Keywords: Na2SiO3, human cancer, antioxidant, HOMO, LUMO

[1]Department of Biotechnology, HST Company, Cairo, Egypt
[2]Faculty Member at Fayoum University, Fayoum University, Fayoum, Egypt
***Correspondence:** hyehia@hlogicgroup.com
Full list of author information is available at the end of article

Introduction

Cancer is often referred to a wide range of diseases characterized by the abnormal growth of cells that divide uncontrollably and could penetrate tissues and destroy healthy tissues in the body and is able to spread throughout the body [1]. Despite significant attempts to develop effective chemotherapy medications, there is still a significant toxicity and selectivity challenges [2,3]. During the human cell life, oxidative damage accumulates despite the presence of the cell's defensive mechanism. Furthermore, the damage caused by radicals to DNA, proteins, and lipids may play a key role in the development of age-related illnesses including cancer, arteriosclerosis, arthritis, neurological disorders, and other health issues [4].

Na_2SiO_3 is utilized as a raw material for a variety of applications, including silica gel, catalyst preparation, medication load, detergent and soap component, refractory ingredient, and deflocculant in clay slurries. The following phases are usually included in the sodium silicate manufacturing process calcination of a combination of sodium carbonate (Na_2CO_3) and natural quartz sand (SiO_2) at 1400-1500 °C in suitable furnaces, according to the reaction

$$Na_2CO_3 + nSiO_2 \rightarrow nSiO_2.Na_2O + CO_2$$

where "n" is the number of sand grains. Under high pressure and temperature, sodium silicate solution was formed in the reaction vessel, and water was evaporated from the silicate solution to produce solid sodium silicate [5,6].

The standard treatment for neoplasias in the early stages includes surgical excision, radiation, chemotherapy, and passive immunotherapy, which uses particular antibodies targeted at neoplastic cells to reduce the total number of tumor cells. Efforts are made to amplify clones of defense cells using appropriate vaccinations in parallel or in the next stage of treatment, which is attracting increasing interest [7]. Cancer affects tens of thousands of patients every year and people are diagnosed with cancer loading to death [8]. The SRB analysis carried out in the cancer of liver (HEPG-2H), breast cancer cells (MCF-7) and blood cancer cells (HCT), revealed that the sodium silicate could effectively reduce the growth and multiplication of the tumor cells. Sodium silicate gel showed better results than solid sodium silicate. Strong scavenging activity by SRB [9]. In addition, it was concluded that the use of an anti-cancer cell culture model showed its effect against the lung carcinoma cell (H1299, A549), liver carcinoma cell line (HEPG-2H), breast carcinoma cell line (MCF7, MDA-MB-231), larynx carcinoma cell line (HEP2), intestinal carcinoma cell line (CACO2) and colon carcinoma cell line (HCT116) were tested by SRB assay. The effective concentration ranged from 125 to 458 µg/ml. DFT calculations were used in studying the binding energies, HOMO-LUMO gap [10,11].

Materials and methods

Human cancer cell lines

The human carcinoma (NCI) cell lines used in this study were obtained from the American Culture Collection (ATCC, MN, USA). Tumor cell lines were maintained at the National Cancer Institute, Cairo, Egypt, by serial subculture.

Drug

Samples were prepared by dissolving 1:1 Stock solution and stored at -20°C in dimethylsulfoxide (DMSO). Different concentrations of the drug were used (Range of concentration used by µg/ml).

Determination of potential cytotoxicity of drug on human cancer cell line

Reagents and buffers

- Glacial acetic acid: 1 % was used for dissolving the unbound SRB dye.
- Sulphorhodamine-B (SRB): 0.4 % concentration was dissolved in 1 % acetic acid was used as a protein dye.
- Trichloroacetic acid (TCA): 50 % stock solution was prepared; 10 % solution was used for protein precipitation.
- Tris base, 10 mM, (pH 10.5) was used for SRB dye solubilization. It was prepared by dissolving 121.1 gm of tris base in 1000 ml distilled water and pH was adjusted by 2 M HCl.

Principle

The cytotoxicity was carried out using sulphorhodamine-B (SRB) assay following the method reported by Skehan., 1990. Sulforhodamine B colorimetric assay is used for cytotoxicity screening. Nat. Skehan., 1990. SRB is a bright pink aminoxanthrene dye with two sulphonic groups. It is a protein stain that binds to the amino groups of intracellular proteins under mildly acidic conditions to provide a sensitive index of cellular protein content.

Procedure

- Cells were seeded in 96-well microtiter plates at initial concentration of $4x10^3$ cell/well in a 200 µl fresh medium and left for 24 hours to attach to the plates.
- Different concentrations (used concentrations) µg/ml of drug was added.
- For each drug concentration, 3 wells were used. The plates were incubated for 48 hours.
- The cells were fixed with 10 µl cold trichloroacetic acid 10% final concentration for 1 hour at 4 0C.
- The plates were washed with distilled water using (automatic washer Tecan, Germany) and stained with 50 µl 0.2 % SRB dissolved in 1 % acetic acid for 30 minutes in dark at room temperature.

- The plates were washed with 1 % acetic acid and air-dried.
- The dye was solubilized with 200 µl/well of 10M tris base (pH 10.5) and optical density (O.D.) of each well was measured spectrophotometrically at 570 nm with an ELISA microplate reader (Sunrise Tecan reader, Germany). The mean background absorbance was automatically subtracted and means values of each drug concentration was calculated.

Calculation

The percentage of cell survival was calculated as follows:

- Surviving fraction = O.D. (treated cells) / O.D. (control cells).
- The IC50 values (the concentrations of drug required to produce 50% inhibition of cell growth) were also calculated using prism version 5.

Computational methods

All computations were carried out using Gaussian 09W hyperchem 8.0, chemcraft 1.6, Gaussview 9.0 and isis draw software package. Molecular geometries of all the studied compounds were fully optimized using B3LYP/6-311G** [12,13]. No symmetry constrains were applied during the geometry optimization [14]. The choice of this basis set was due to its flexibility and the fact that the diffused p functions on the H-atom tend to compensate the inharmonic effects of the CH and NH stretches. By using HOMO and LUMO energy values for a molecule, using RHF/6-311G**, electronegativity and chemical hardness can be calculated as follows:

X = (I+A)/2 (electronegativity), η = (I-A)/2 (chemical hardness), S = 1/2η (chemical softness),

where I and A are ionization potential and electron affinity, and I = -EHOMO and A = -ELUMO, respectively [15]. Throughout this work, MOs were constructed using the Gauss-view 5.08 visualization program. The total static dipole moment (µ), the mean polarizability <α>, the anisotropy of the polarizability Δα and the mean first hyper polarizability <β> using the x, y, z components were calculated by using the following equations [15]:

$$\mu = \left(\mu_x^2 + \mu_y^2 + \mu_z^2\right)^{\frac{1}{2}}$$

$$\alpha = \frac{(\alpha_{xx} + \alpha_{yy} + \alpha_{zz})}{3}$$

$$\Delta\alpha = \left(\left(\alpha_{xx} - \alpha_{yy}\right)^2 + \left(\alpha_{yy} - \alpha_{zz}\right)^2 + (\alpha_{zz} - \alpha_{xx})^2/2\right)^{\frac{1}{2}}$$

$$\langle\beta\rangle = (\beta_x^2 + \beta_y^2\beta_z^2)^{\frac{1}{2}}$$

where

$$\beta_x = \beta_{xxx} + \beta_{xyy} + \beta_{xzz}$$
$$\beta_y = \beta_{yyy} + \beta_{xxy} + \beta_{yzz}$$
$$\beta_z = \beta_{zzz} + \beta_{xxz} + \beta_{yyz}$$

Anticancer activity

Human Hepatoma (HepG2) Cells and Ehrlich Ascites Carcinoma (EAC) cell lines were prepared from National cancer institute, Cairo, Egypt. The cancer cells were cultured in HCT, HEPG2-H and MCF7-H medium and supplemented with 10% FBS, 100U/ml penicillin, 100 µg/ml streptomycin, and ٢mML-glutamine incubated at ٣٧°C for 24hrs with 5% CO_2 in air [16]. 0.005 to 0.125 mg/ml in methanol and expressed as mg of Quercetin equivalents.

Results

The anticancer activity of nano-sodium silicate was examined against cancer cell lines (H1299, A549, MCF7, MDA-MB-231, HEPG2, HEP2, CACO2, and HCT116, respectively). Applied samples at IC50 concentrations ranged from 0.0 to 500.0 µg/ml.

The epithelial lung cell cancer and human larynx epithelioma cancer in the form of A549, HEP2 and H1299 cells line exhibited more resistance for sodium silicate gel and there were appeared clearly in the value of lC50 which recorded (125, 148 and 167 µg/ml) (**Fig. 1-3**). Breast cancer is cancer that develops from breast tissue [17]. Signs of breast cancer may include a lump in breast, a change in breast shape and dimpling of the skin [18].

Moreover, the different concentration of samples gel showed sharply decrease in LC50 comparison to the other concentration of solid's samples against cancer cells lines, MCF7 and MDA-MB-231 (**Fig. 4, 5**). The best results were recorded in MCF7-1 cell line (187 µg/ml); this was appeared clearly in the value e of LC50.

On the other hand, the intestinal epithelial barrier cancer in the form of (CACO2) cell line exhibited more resistance for gel samples, and this was appeared clearly in the value of LC 50 which recorded 213 µg/ml (**Fig. 6**) compared with solid samples who appeared clearly in the value of LC 50 which recorded 430 µg/ml, Hematopoietic cell transplantation (HCT) is the intravenous injection of a hematopoietic stem. The study indicates that the gel sample is vulnerable against cancer cells while it is non-toxic to normal cells. The data (**Fig. 7, 8**) indicate that sodium silicate nanoparticles can prevent carcinogenesis with a LC value of 50 that recorded 218 µg/ml. Moreover, this study to determine the antiproliferative effects of sodium silicate nanoparticles on hepatocellular carcinoma, HepG2, was the IC value of the gel sample towards HepG2 which scored 228 µg/ml better than the solid sample which scored 418 µg/ml [19].

Discussion

In **figure 9** Nayak et al. (1998) explored the geometries of the Si_3Om_2 (m51,4,6) clusters. While the geometries of the anions remain similar to those of neutral clusters, the bond lengths especially in Si_3O_{42} and Si_3O_{62} do differ from the neutral clusters. More importantly, the Mulliken charge distribution in anionic clusters differs substantially from those in the neutral clusters [20]. For example, in Si_3O_2 almost as much negative charge resides on one of the Si atoms as on the oxygen atom. On the other

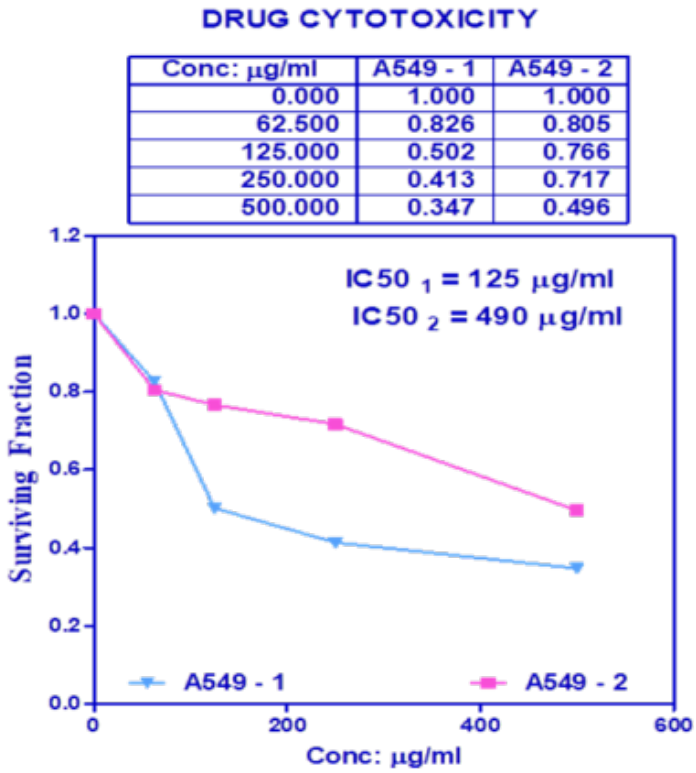

FIGURE 1 The effect of the difference between sodium silicate gel and sodium silicate solids on the survival of part of the lung tissue

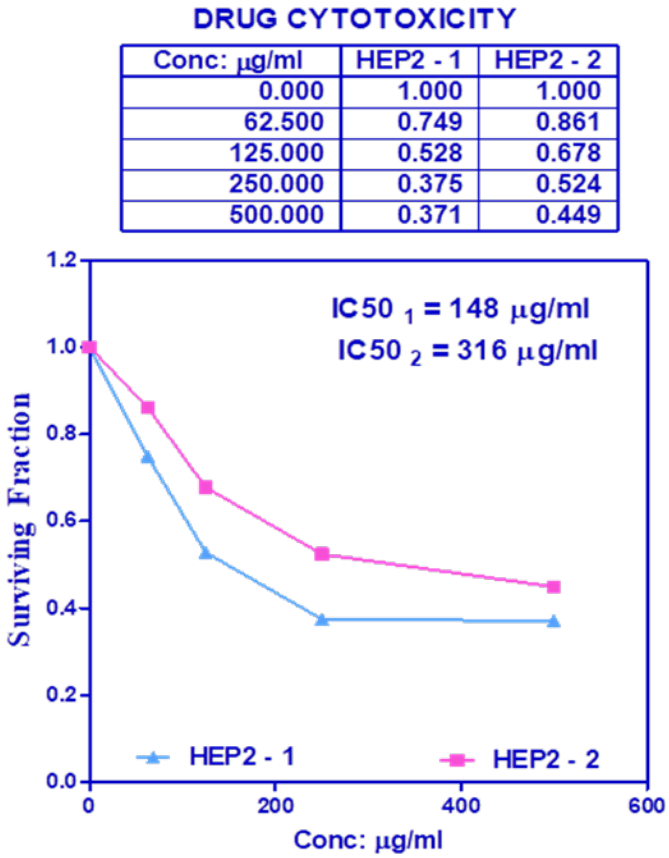

FIGURE 2 The effect of the difference between sodium silicate gel and sodium silicate solids on the survival of part of the larynx

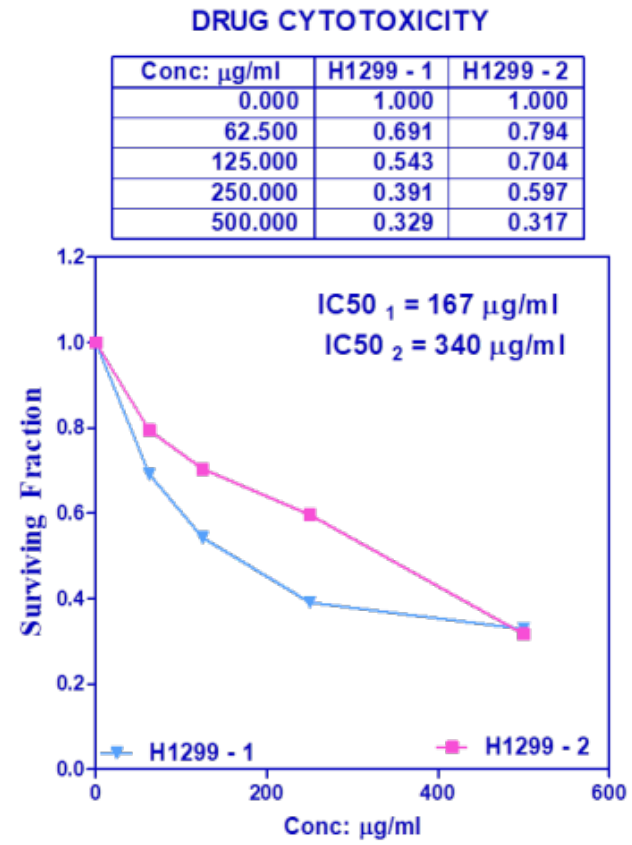

FIGURE 3 The effect of the difference between sodium silicate gel and sodium silicate solids on the survival of part of the lung

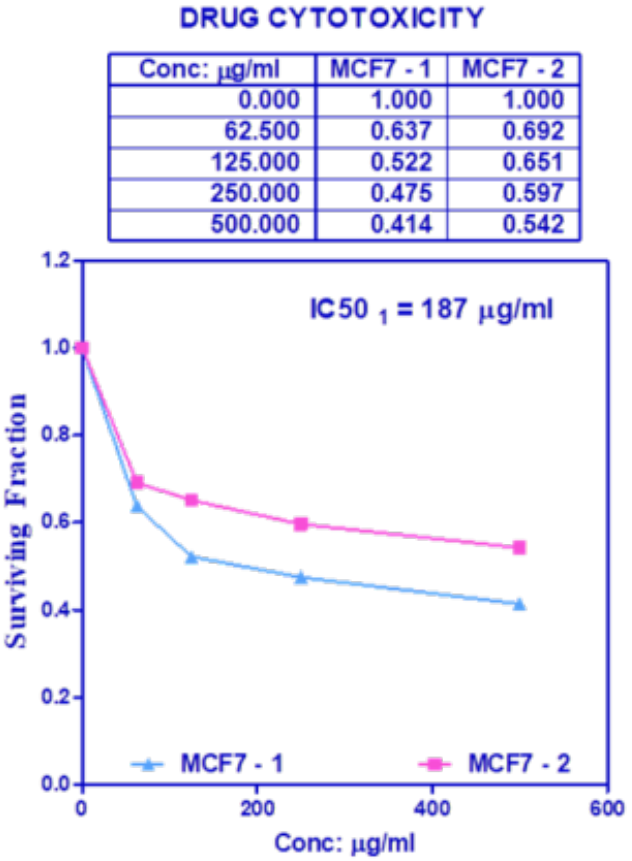

FIGURE 4 The effect of the difference between sodium silicate gel and sodium silicate solids on the survival of part of the breast

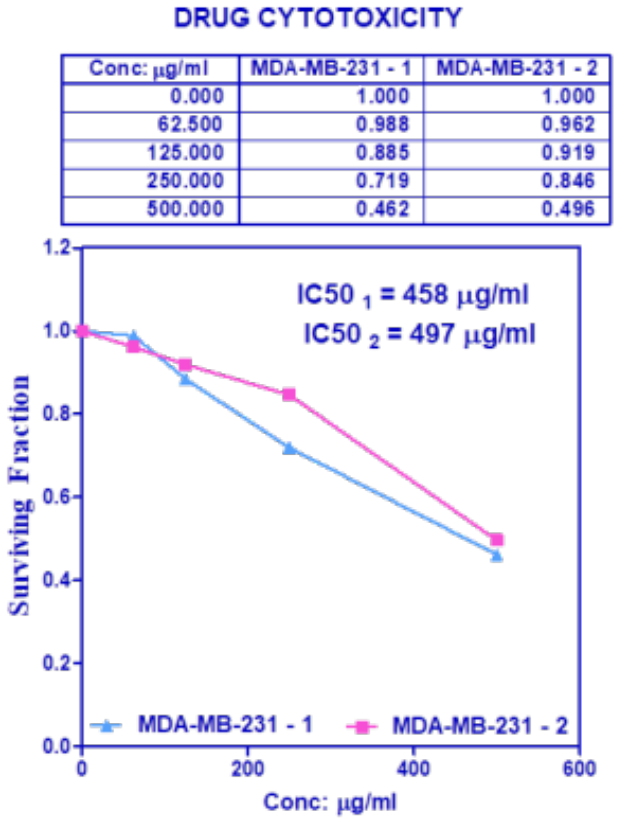

FIGURE 5 The effect of the difference between sodium silicate gel and sodium silicate solids on the survival of part of the breast

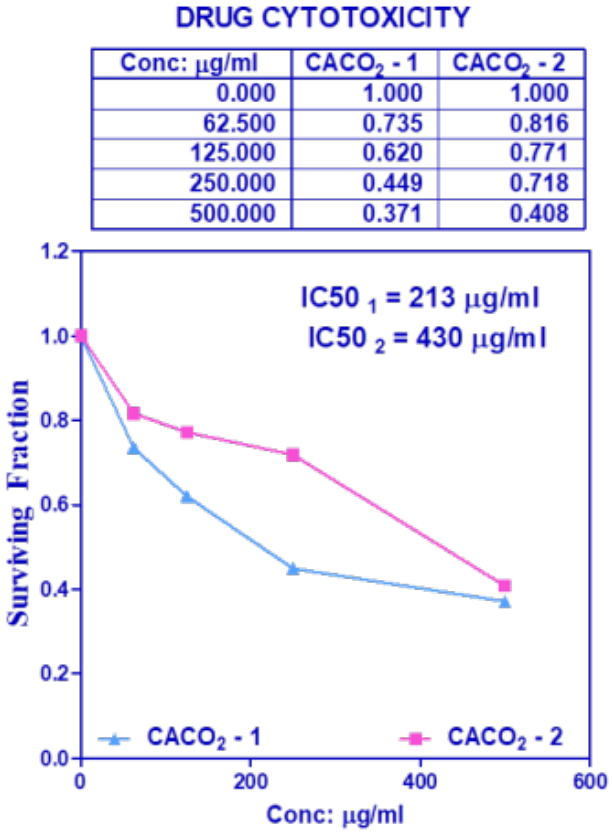

FIGURE 6 The effect of the difference between sodium silicate gel and sodium silicate solids on the survival of part of the intestinal

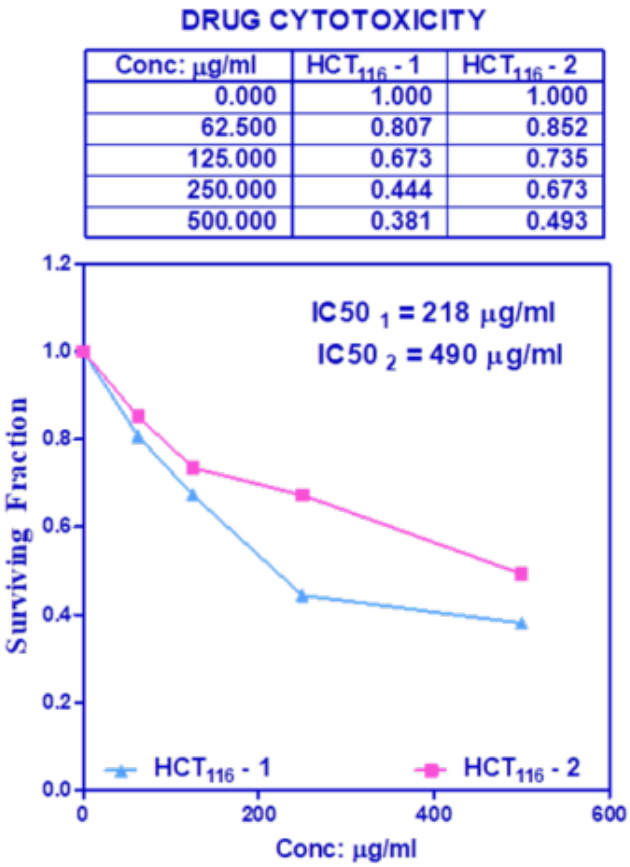

FIGURE 7 The effect of the difference between sodium silicate gel and sodium silicate solids on the survival of part of the colon

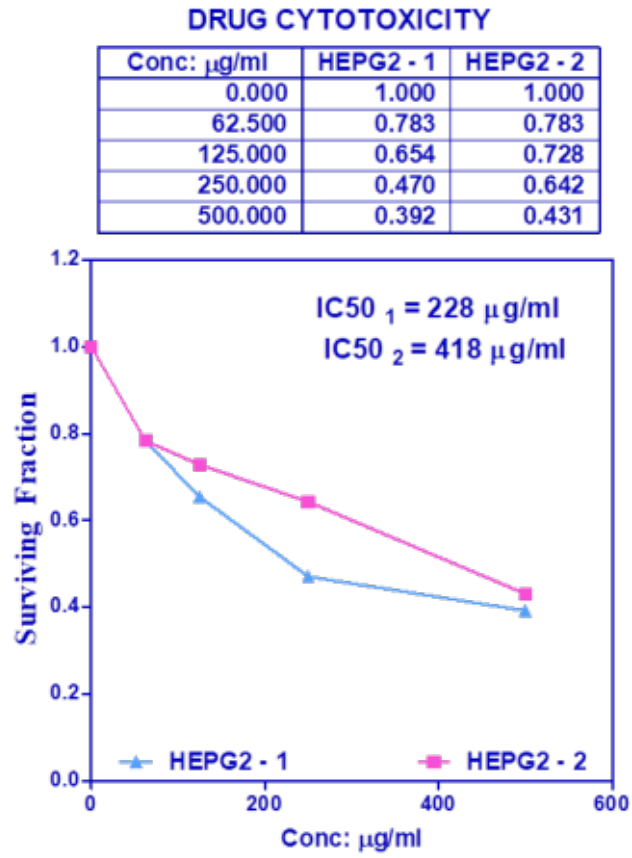

FIGURE 8 The effect of the difference between sodium silicate gel and sodium silicate solids on the survival of part of the liver

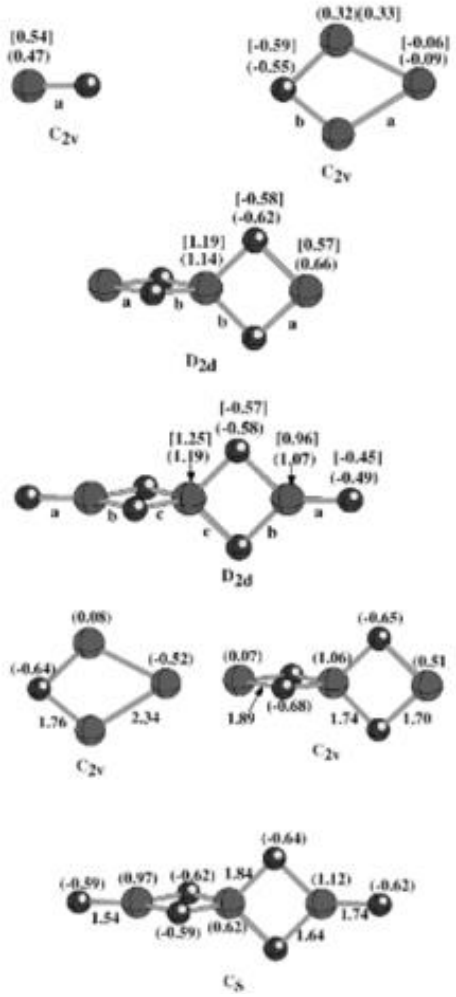

FIGURE 9 Equilibrium geometries of neutral SiO, Si_3O_m (m51,4,6) clusters using GAUSSIAN 94 and DMOL codes. Small dark balls represent O atom and large gray balls represent Si atom. Mulliken charges on various atoms are shown in the figure

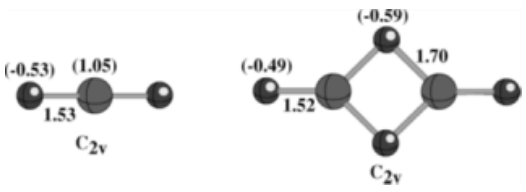

FIGURE 10 Equilibrium structures of SiO_2 and $(SiO_2)_2$

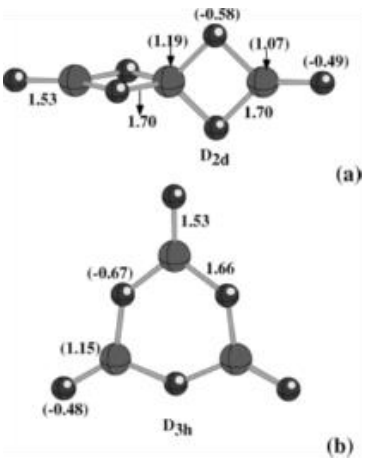

FIGURE 11 Geometries of $(SiO_2)_3$ cluster corresponding to the ground state and two higher energy configurations

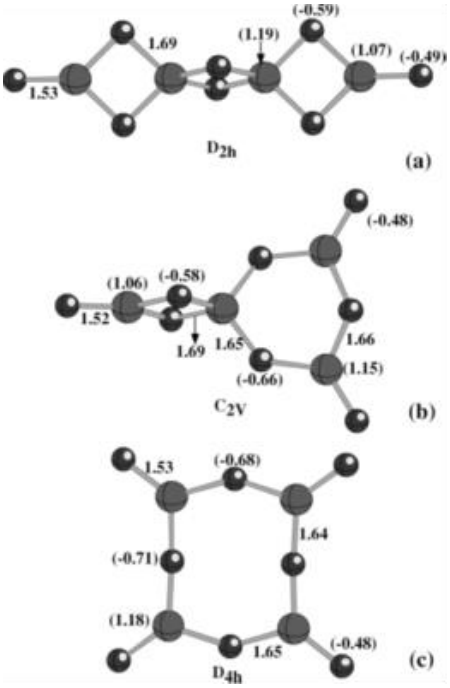

FIGURE 12 Ground state geometry and the next higher energy isomers of $(SiO_2)_4$ clusters. See the text for details

hand, in Si_3O_{42} and Si_3O_{62} clusters, no Si atom carries a negative charge. On the other hand, in Si_3O_4 and Si_3O_6 clusters, no Si atom carries a negative charge.

In **figure 9** Nayak et al. (1998) compared the binding energies, ionization potentials, and electron affinities calculated using GAUSSIAN 94 and DMOL codes with available experimental and MP2 results. For SiO both theories yield binding energies in good agreement with experiment. The vertical and adiabatic electron affinities agree very well with both MP2 and experimental results. There are no measured vertical ionization potentials of Si_3Om (m51,4,6), but our value for SiO again agrees very well with experiment [21]. Thus, we conclude that the density functional theory at the GGA level can provide reliable results. We have also repeated the vertical and adiabatic electron affinity calculations of Si_3O_4 using the Vosko-Wills-Nusair form for the local density approximation in the GAUSSIAN 94 code [21]. While this comparison might indicate that LDA may be just as good as GGA level of theory, we have carried out the remaining calculations using the GGA.

Since these potentials were developed for bulk systems and lack directional dependence, we have calculated the equilibrium geometries of the ground state and higher energy isomers using the GAUSSIAN 94 and the GGA level of theory [22]. We have optimized several structural forms to obtain the lowest energy structures [23]. We begin with the geometry of SiO_2 cluster. Analogous to the CO_2 molecule, the geometry of SiO_2 is linear with an Si–O bond length of 1.53 Å and a binding energy of 8.06 eV. We define the binding energy as the energy necessary to dissociate the cluster into separated atoms. While our calculated bond length is reasonably close to the 1.46 Å value obtained by Nayak et al. (1998), our binding energy differs substantially from their value of 44.73 eV. The Mulliken charge on the Si and O atoms are indicated in parentheses in **figure 10**. A net charge of 11.05 on Si and 20.53 on O is indicative of partial ionic bonding in SiO_2.

This trend continues as SiO_2 clusters grow. The ground state geometry of $(SiO_2)_2$ in **figure 10** has a planar C2v structure with 1A1 electronic state. The O atoms form a symmetric structure. The bond length between Si and O atoms forming a double bridge between Si atoms is elongated compared to the bond between the external O atom with Si. As we will see in the following this trend continues as trimers and higher clusters of SiO_2 form. The charge on the O atoms and Si atoms remain fairly close to their value in the SiO_2 monomer. This indicates that partial ionic bonding continues with increasing silica cluster size. This is in contrast to clusters of CO_2. For example, the binding in $(CO_2)_2$ is of weak van der Waals character. The binding energy of the $(SiO_2)_2$ dimer against the separated SiO_2 monomer is 3.67 eV which again differs significantly from the empirical potential calculation of Manoj Kumar et al. (2020) study [20].

The geometries of the $(SiO_2)_3$ isomers are shown in **figures 11, 12**. Nayak et al. [21] have identified two structures of $(SiO_2)_3$: a planar ring structure with D3h symmetry and a three-dimensional structure with D2d symmetry where four O atoms belong to double bridges and two end O atoms bonded to Si atoms [21-23]. The authors found the D3h structure to be lower in energy from the D2d structure by 0.43 eV. Our results are just the opposite. We find the D2d structure to be the ground state which

lies 0.69 eV lower in energy from the D3h structure. This can be explained by examining the coordination of the individual Si and O atoms. We note that Si is tetravalent, and O is divalent. Thus, ideally in each cluster structure, Si and O would, respectively [24].

Generally, the inhibition on different cancer cells increase gradient by increasing extract concentration [25]. Conclusively, the effective concentration was ranged from 125 to 458 µg/ml, this effect may be due to sodium silicate nanoparticles. These data have been adapted by Pasternak et al. [18]. HOMO-LUMO gap decreases with increase Oxygen deficiency. This could explain the new optical properties of silica nanoparticles. More experimental and Theoretical work on silica groups with varying oxygen concentration It will be very useful [10].

Conclusions

Due to the toxicity of current chemotherapy and cancer cell resistance to anticancer medications, this study is seeking for innovative therapeutics and prevention techniques. Density-functional theory calculations under the B3LYP/6-311G** level was used to explore the structural and molecular properties of sodium silicate nanoparticles. The study was concerned with the engineering properties and different molecular recipes such as HOMO, LUMO and Egap in order to determine the arrangement of molecules as a powerful antioxidant and thus most of the compounds act as anticancer [14,15]. We found that sodium silicate gel particles are responsible for the antioxidant activity so it can be used as an antioxidant and anticancer for prevention and treatment. Through these results, we can say that it is possible to overcome some of the negative effects of chemotherapy for cancer patients by using natural substances i.e., Na_2SiO_3 that have the ability to transfer the drug and raise alkalinity rates, which contributes to the treatment of cancer in human cells.

Ethical approval

The trial protocol is then reviewed by a Research Ethics Committee of the National Cancer Institute of Egypt. Respect for the rights and dignity of participants, including confidentiality and anonymity.

Acknowledgements

The authors extend their sincere thanks to the work team at the National Cancer Institute of Egypt for allowing us to conduct analyzes and experiments inside the institute's laboratories.

Corresponding author

Hesham Mohamed Abdal-Salam Yehia, Department of Biotechnology, HST Company, Tayaran St, 11765, Cairo, Egypt, e-mail: hyehia@hlogicgroup.com.

Conflict of interest statement

The authors declare no conflict of interest.

References

1. Falzone L, Salomone S, Libra M. Evolution of cancer pharmacological treatments at the turn of the third millennium. Front Pharmacol. 2018;9:1300; DOI:10.3389/fphar.2018.01300.
2. Eken A, Erdem O, Arsova-Sarafinovska Z, Akay C, Sayal A, Matevska N, Suturkova L, Erten K, Ozgok Y, Dimovski A, Aydin A. Association between gene polymorphism of manganese superoxide dismutase and prostate cancer risk. J Biochem. 2013;27(3):213-8; DOI:10.1002/jbt.21472.
3. Avcı, D., Başoğlu, A. & Atalay, Y. Ab initio HF and DFT calculations on an organic non-linear optical material. Struct Chem. 2010;21(1):213–219; DOI:10.1007/s11224-009-9566-1.
4. Sonia E. Ulic, Carlos O. Della Védova, Angelika Hermann, Hans-Georg Mack, and Heinz Oberhammer. J Phys Chem. 2008:112(27):6211-621; DOI:10.1021/jp800344m.
5. Yehia HM, Said SM. Effects of the addition of titanium dioxide; sodium silicate and silica nanoparticles on the elimination of bacteria and viruses in a physical field. Am J Biomed Res. 2021;9(2):24-29; DOI:10.12691/ajbr-9-2-1.
6. Yehia HM, Said SM. Drinking water treatment: pH adjustment using natural physical field. J Biosci Med. 2021;9(6):55-66; DOI:10.4236/jbm.2021.96005.
7. Kawiak J, Hoser G, Domagała-Kulawik J. Problems of cancer treatment. Part 2. Treatment based on modification of anticancer immunological responses in therapy. Med J Cell Biol. 2017;5(1):96-112; DOI:10.1515/acb-2017-0007.
8. Daniyal M, Siddiqui ZA, Akram M, Asif HM, Sultana S, Khan A. Epidemiology, etiology, diagnosis and treatment of prostate cancer. APJCP. 2014;15(22):9575-8. DOI:10.7314/APJCP.2014.15.22.9575.
9. Saw, C.LL., Wu, Q. & Kong, AN. Anti-cancer and potential chemopreventive actions of ginseng by activating Nrf2 (NFE2L2) anti-oxidative stress/anti-inflammatory pathways. Chin Med. 2010;5:37; DOI:10.1186/1749-8546-5-37.
10. Lin D, Xiao M, Zhao J, Li Z, Xing B, Li X, Kong M, Li L, Zhang Q, Liu Y, Chen H. An overview of plant phenolic compounds and their importance in human nutrition and management of type 2 diabetes. Molecules. 2016;21(10):1374. DOI:10.3390/molecules21101374.
11. Elmore JG, Armstrong K, Lehman CD, Fletcher SW. Screening for breast cancer. Jama. 2005;293(10):1245-56; DOI:10.1001/jama.293.10.1245.
12. Yismaw, S., Ebbinghaus, S.G., Wenzel, M, Poppitz D, Glaser R, Matysik J, Bauer F, Enke D. Selective functionalization of the outer surface of MCM-48-type mesoporous silica nanoparticles at room temperature. J Nanopart Res. 2020;22:279; DOI:10.1007/s11051-020-05006-2.
13. Xie F, Ye L, Ta M, Zhang L, Jiang WG. MTSS1: a multifunctional protein and its role in cancer invasion and metastasis. Front Biosci. 2011;3(2):621-31; DOI: 10.2741/s175.
14. Skehan P, Storeng R, Scudiero D, Monks A, McMahon J, Vistica D, Warren JT, Bokesch H, Kenney S, Boyd MR. New colorimetric cytotoxicity assay for anticancer-drug screening. J Natl Cancer Inst. 1990;82(13):1107-12; DOI:10.1093/jnci/82.13.1107.
15. Aziz AA, Elantabli FM, Moustafa H, El-Medani SM. Spectroscopic, DNA binding ability, biological activity, DFT calculations and non linear optical properties (NLO) of novel Co (II), Cu (II), Zn (II), Cd (II) and Hg (II) complexes with ONS Schiff base. J Mol Struct. 2017;1141:563-76; DOI:10.1016/j.molstruc.2017.03.081.
16. Atalay Y, Avcı D, Başoğlu A. Linear and non-linear optical properties of some donor–acceptor oxadiazoles by ab initio Hartree-Fock calculations. Struct Chem. 2008;19:239–246; DOI:10.1007/s11224-007-9278-3.
17. Jemal A, Bary F, Center MM, Ferley J, Ward E, Forman D. Global cancer statistics. CA Cancer J Clin. 2011;61(2):69-90; DOI: 10.3322/caac.20107.
18. Pasternak K, Nowacka O, Wróbel D, Pieszyński I, Bryszewska M, Kujawa J. Influence of MLS laser radiation on erythrocyte membrane fluidity and secondary structure of human serum albumin. Mol Cell Biochem. 2014;388:261–267; DOI:10.1007/s11010-013-1917-y.
19. Zhou W, Li X, Liu F, Xiao Z, He M, Shen S, Liu S. MiR-135a promotes growth and invasion of colorectal cancer via metastasis suppressor 1 in vitro. Acta Biochem Biophys Sin. 2012;44(10):838-46; DOI:10.1093/abbs/gms071.
20. Manoj Kumar P, Mylsamy K, Saravanakumar PT. Experimental investigations on thermal properties of nano-SiO2/paraffin phase change material (PCM) for solar thermal energy storage applications. Energy Sources A: Recovery Util. Environ. Eff. 2020;42(19):2420-33; DOI:10.1080/15567036.2019.1607942.
21. Nayak SK, Rao BK, Khanna SN, Jena P. Atomic and electronic structure of neutral and charged Si n O m clusters. J. Chem. Phys. 1998;109(4):1245-50; DOI:10.1063/1.476675.
22. Frixen UH, Behrens J, Sachs M, Eberle G, Voss B, Warda A, Löchner D, Birchmeier W. E-cadherin-mediated cell-cell adhesion prevents invasiveness of human carcinoma cells. The J Cell Biol. 1991;113(1):173-85; DOI:10.1083/jcb.113.1.173.

23. Maier G, Reisenauer HP, De Marco M. Isonitroso hydrogen (Hydroxy nitrene, HON). Angew. Chem. Int. Ed. 1999;38(1-2):108-10; DOI: 10.1002/(SICI)1521-3773(19990115)38:1/2<108::AID-ANIE108>3.0.CO;2-U
24. Al-Fahad D, Alharbi BF, Bih CI, Dash PR. Nitric oxide may regulate focal adhesion tu rnover and cell migration in MDA-MB-231 breast cancer cells by modulating early endosome trafficking. Med J Cell Biol. 2021;9(2):60-72. DOI:10.2478/acb-2021-0010.
25. Moliner V, Escribano P, Peris E. Intermolecular hydrogen bonding in NLO. Theoretical analysis of the nitroaniline and HF cases. New J. Chem. 1998;22:387-392 DOI:10.1039/A708755A